Acta Oceanol. Sin., 2018, Vol. 37, No. 7, P. 105–117
DOI: 10.1007/s13131-017-1248-7
http://www.hyxb.org.cn
E-mail: hyxbe@263.net

The dynamic observation of dissolved organic matter in the Zhujiang (Pearl River) Estuary in China from space

LIU Dong[1, 2], BAI Yan[1]*, HE Xianqiang[1], PAN Delu[1], WANG Difeng[1], WEI Ji'an[1], ZHANG Lin[1]

[1] State Key Laboratory of Satellite Ocean Environment Dynamics, Second Institute of Oceanography, State Oceanic Administration, Hangzhou 310012, China

[2] Key Laboratory of Watershed Geographic Sciences, Nanjing Institute of Geography and Limnology, Chinese Academy of Sciences, Nanjing 210008, China

Received 14 June 2017; accepted 2 November 2017

Abstract

The distributions of estuarine colored dissolved organic matter (CDOM) are the combined results of physical-biogeochemical processes. Remote sensing is needed to monitor highly dynamically estuarine CDOM. Using *in situ* data from four seasonal cruises, an algorithm is developed to estimate CDOM absorption coefficient at 400 nm ($a_{CDOM}(400)$) in the Zhujiang (Pearl River) Estuary (ZJE). The algorithm uses band ratios of $R_{rs}(667)/R_{rs}(443)$ and $R_{rs}(748)/R_{rs}(412)$. By applying it to moderate resolution imaging spectroradiometer onboard Aqua satellite (MODIS/Aqua) data from 2002 to 2014, seasonal climatology $a_{CDOM}(400)$ in the ZJE is calculated. CDOM distributions are majorly influenced by water discharge from the Zhujiang River and underwater topography. Along the section vertical to a water depth gradient, the seasonal $a_{CDOM}(400)$ exponentially decreased ($y=ae^{bx}$, $b<0$), but with great differences among seasons. Riverine fresh water is the primary source of CDOM in the ZJE. Fulvic acid fraction decreases with increasing salinity. Using developed algorithms, conservative CDOM mixing equation, and river discharge, effective riverine end-member concentration and flux of dissolved organic carbon (DOC) in summer and winter from 2002 to 2014 are first estimated from the MODIS/Aqua data. Both effective riverine end-member DOC concentration and flux are positively related to the river discharge, significantly in summer with R^2 of 0.698 for concentration and 0.965 7 for flux.

Key words: colored dissolved organic matter, dissolved organic carbon, Zhujiang (Pearl River) Estuary, effective riverine end-member flux, remote sensing

Citation: Liu Dong, Bai Yan, He Xianqiang, Pan Delu, Wang Difeng, Wei Ji'an, Zhang Lin. 2018. The dynamic observation of dissolved organic matter in the Zhujiang (Pearl River) Estuary in China from space. Acta Oceanologica Sinica, 37(7): 105–117, doi: 10.1007/s13131-017-1248-7

1 Introduction

The global lateral flux of dissolved organic matter (DOM), determined as dissolved organic carbon (DOC) and hereinafter, into estuaries by rivers was estimated at 210 Mt/a (calculated by carbon) (Dai et al., 2012). Phytoplankton production and sediment pore water can also add DOM to estuarine waters. Riverine or autogenous DOM can influence toxic metal transport, oxygen consumption, etc. (Dai et al., 2012; Chen et al., 2013; Guo et al., 2013) so as to change estuarine water quality. Moreover, the optically active DOM fraction, colored dissolved organic matter (CDOM), can absorb light especially for that with short wavelength (Chen et al., 2004, 2013; Huang and Chen, 2009). As results, CDOM may increase primary production by absorbing harmful ultraviolet light on the one side, or reduce photosynthetic production in deep waters due to limitation of photosynthetic active radiation on the other (Huang and Chen, 2009). Therefore, monitoring CDOM distribution and its composition have great significance to estuarine water resource management. Except for CDOM, moreover, non-colored DOM can also influence estuarine carbon cycle, oxygen consumption, etc. (Dai et al., 2012; Chen et al., 2013; Guo et al., 2013).

Estuarine CDOM concentration, determined as light absorption coefficient at a specific wavelength, can be monitored from space in high tempo-spatial resolution using band ratio algorithm (Carder et al., 2003; Park et al., 2014; Siegel et al., 2002; Siswanto et al., 2011). Tiwari and Shanmugam (2011) recommended a linear equation using the ratio of remote sensing reflectance at 670 and 490 nm ($R_{rs}(670)/R_{rs}(490)$) to derive CDOM in both coastal and open ocean waters. For waters influenced by the Mississippi River during low flow conditions, D'sa and Miller (2003) reported that power law equation using the ratio of remote sensing reflectance at 510 and 555 nm ($R_{rs}(510)/R_{rs}(555)$) was the best CDOM inversion algorithm. However, these algorithms were not very appropriate for all kinds of waters with

Foundation item: The National Key Research and Development Progam of China under contract No.2017YFA0603003; the National Basic Research Program (973 Program) of China under contract No. 2015CB954002; the Public Science and Technology Research Funds Project of Ocean under contract No. 201505003; the National Natural Science Foundation of China under contract Nos 41676170, 41676172, 41476155, 41621064 and 41406202; the Project of State Key Laboratory of Satellite Ocean Environment Dynamics, Second Institute of Oceanography, State Oceanic Administration of China under contract No. SOEDZZ1801;the Research Startup Project of Nanjing Instiute of Geography and Limnology, Chinese Academy of Sciences under contract No. Y7SL051001.
*Corresponding author, E-mail: baiyan@sio.org.cn

various inherent optical properties because of different constituents (Sathyendranath, 2000). Local algorithm should be developed to inverse estuarine CDOM accurately. For remote sensing monitoring of CDOM in the Zhujiang (Pearl River) Estuary (ZJE), Chen et al. (2003) first used $R_{rs}(670)/R_{rs}(412)$ to inverse CDOM from simulated water reflectance from suspended particle, chlorophyll *a* (Chl *a*) and DOC concentrations. Based on *in situ* CDOM and Hyperion satellite data, Fang et al. (2009) also reported a weak relationship between CDOM and $R_{rs}(703)/R_{rs}(488)$. By using *in situ* data and extending the quasi-analytical algorithm (QAA) (Lee et al., 2002), Dong et al. (2013) recently derived the absorption coefficient of CDOM in the South China Sea and the Taiwan Strait close to the ZJE. From our *in situ* data in the ZJE, however, we got that all of these algorithms did not perform well for the local ZJE.

A great amount of DOM was discharged into the ZJE by the Pearl River, the 14th largest world river with discharge of about 343 km^3/a (Cai et al., 2008). Riverine DOC flux was calculated by multiplying river discharge by average DOC concentration over a given time period (Bauer et al., 2013). However, the DOC concentration spatially varies along the river stream (Wu et al., 2007). Gao et al. (2002) estimated DOC flux at the Makou Hydrometric Station of the Xijiang River, accounting for 78% of drainage area of the Zhujiang River, to be 0.66 Mt C/a (calculated by carbon). Ni et al. (2008) reported the total DOC flux at eight outlets of the Zhujiang River to be 0.38 Mt/a using *in situ* data sampled monthly from March 2005 to February 2006. This estimation could denote annual riverine DOC flux into the ZJE. Once entering the estuary, however, there were rapid transformations from riverine DOC to particulate organic carbon (POC) through flocculation (Bauer et al., 2013) and from riverine POC to DOC through microbial activities (Dai et al., 2000) in the low salinity waters. Therefore, an effective riverine end-member DOC concentration was defined to denote the resultant riverine DOC after various transformations in low salinity waters (Section 4.3) (Cai et al., 2004).

In this study, remote sensing algorithms for inversing CDOM absorption coefficient at 400 nm ($a_{CDOM}(400)$) and its spectral slope (S_{CDOM}) were developed using synchronous *in situ* water reflectance spectra and CDOM data from four seasonal survey cruises in the ZJE firstly. Then, the developed algorithms were applied on moderate resolution imaging spectroradiometer onboard Aqua satellite (MODIS/Aqua) data to calculate a seasonal climatology $a_{CDOM}(400)$ and S_{CDOM} in the ZJE. Thirdly, effective riverine end-member DOC fluxes in summer and winter from 2002 to 2014 were also estimated from the MODIS/Aqua data. Furthermore, we also discussed CDOM dynamics including its sources, impact factors, and distributions in the ZJE. In short, using the developed algorithms, CDOM dynamics in the ZJE can be monitored in high tempo-spatial resolution from space.

2 Study area

ZJE receives fresh water from the second largest China's river, the Zhujiang River, ranked after the Changjiang River and before the Huanghe River according to annual discharge (Cai et al., 2008). Fresh water is discharged into the ZJE through eight outlets, Humen, Jiaomen, Hongqili, Hengmen, Modaomen, Jitimen, Hutiaomen and Yamen (Fig. 1b). The Zhujiang River Basin is located in the subtropical zone and affected by the East Asian Monsoon. Annual fresh water from the Zhujiang River is unevenly seasonally distributed. About 80% of fresh water from the Zhujiang River occurs during the wet season from April to September, with only 20% happens in the dry season from October to March (Chen et al., 2004; Bai et al., 2015). The total suspended matter (TSM) concentration is high in the ZJE, especially for the near shore waters. On the one hand, the Zhujiang River is the 14th largest world river (Cai et al., 2008), with annual discharge of 343 km^3/a. Under the influence of the East Asian Monsoon, it discharges more highly turbid water than Europe and America rivers into the ZJE (Ran et al., 2013). On the other hand, suspen-

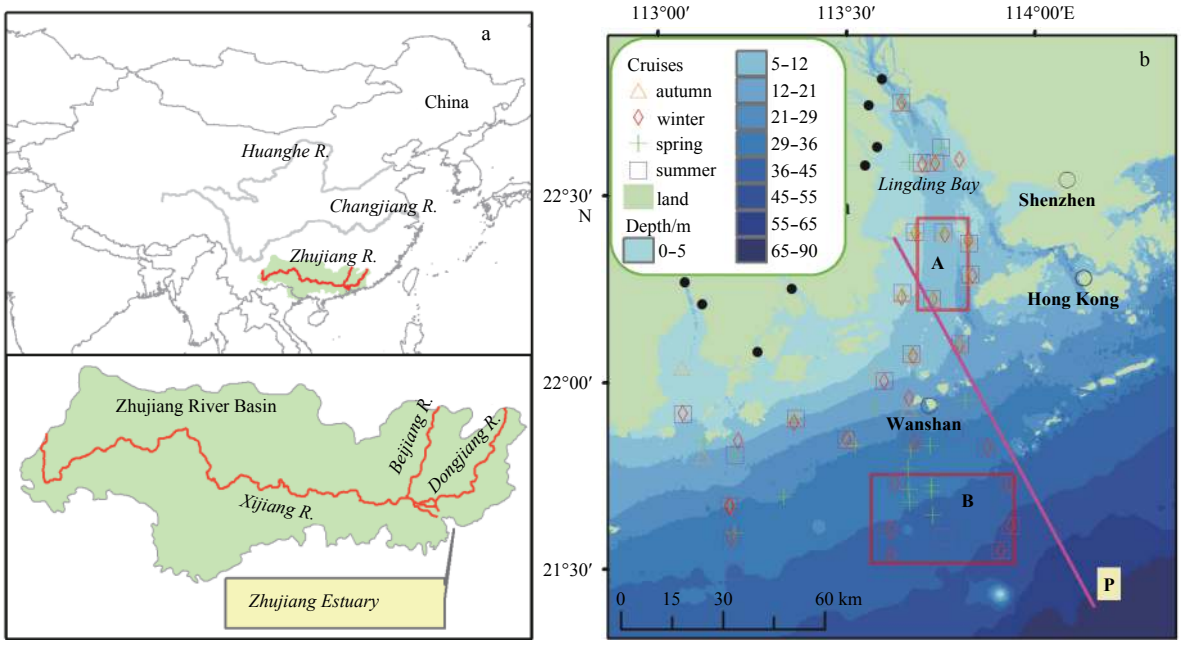

Fig. 1. The studied estuary and its related river basin. a. Schematic map of the Zhujiang River; and b. sampling sites in the ZJE. The rectangle A defines a region with the low salinity waters, and the rectangle B with high salinity waters. Line P shows a section vertical to the water depth gradient ranging from (22°23.056′N, 113°36.914′E) to (21°23.864′N, 114°8.538′E). Major cities or towns around the ZJE are symbolized by unfilled circles (○). River outlets are denoted by filed circles (●).

ded matter can scatter sun light and increase water reflectance. Most of *in situ* R_{rs}(490) used by D'sa and Miller. (2003) from the Gulf of Mexico, Tiwari and Shanmugam (2011) from global coastal oceans were smaller than 0.01 sr^{-1}. However, 55 of the 67 *in situ* R_{rs}(490) in the ZJE from our cruises were larger than 0.01 sr^{-1}.

The DOM concentration intensely varied in the ZJE, with a_{CDOM}(400) as high as 1.134 m^{-1} in the low salinity waters and only 0.04 m^{-1} in the high salinity waters. The ZJE connects the Zhujiang River to the SCS. The part north of Wanshan is also called as the Lingding Bay. The topography of the Lingding Bay presents as high in the west and low in the east (Fig. 1b). Most fresh water is discharged into the ZJE from the shallowly west side, where all outlets of the Zhujiang River are located. However, along the two eastern water channels saline waters can intrude into the ZJE from the deeply east part when tiding, even into the northernmost outlet at high tide (Fig. 1b) (Liu et al., 2015). As a result of interactions between fresh and saline waters, a counterclockwise flow can be observed in the Lingding Bay (Chen et al., 2004). The area south of Wanshan is significantly influenced by coastal currents along Guangdong Province, China. DOM dynamics are the combined results of various physical-biogeochemical processes in the ZJE (Callahan et al., 2004; Chen et al., 2004; He et al., 2010).

3 Materials and ZJE processing

3.1 *In situ data*

3.1.1 *CDOM and DOC*

Four seasonal survey cruises were conducted in autumn (November 2013), winter (February 2014), spring (May 2014), and summer (August 2014) in the ZJE. Sampling sites in different cruises are shown in Fig. 1b. CDOM samples were collected following the Ocean Optics Protocols proposed by the NASA (Mitchell et al., 2000). Surface water was collected using a Niskin water sampler (General Oceanics Inc, USA), stored in brown glass bottles until filtration so as to keep away from sun light (Liu et al., 2015), filtrated on board through polycarbonate filters (millipore, 0.22 μm, and Φ 47 mm) at a low vacuum around 125 mm-Hg (Bai et al., 2013). The CDOM samples were strained straightly into CNW™ brown glass bottles with teflon gaskets. All CNW™ bottles had been soaked in 10% HCl, rinsed with purified Milli-Q water, and combusted at 450°C for 4 h (Bai et al., 2013). After collection, the CDOM samples were immediately placed into a refrigerator with temperature around –20°C until laboratory measurement (Bai et al., 2013; Liu et al., 2014). Ranging from 250 to 800 nm with an interval of 1 nm, the light absorbance of CDOM sample (OD_{CDOM}) and purified Milli-Q water ($OD_{Milli\text{-}Q}$) were both measured using a Lambda 35 ultraviolet-visible light spectrophotometer (Perkin Elmer, Inc). Then, the CDOM absorption coefficient at a specific wavelength λ ($a_{CDOM}(\lambda)$) was calculated using Eq. (1) (Bai et al., 2013).

$$a_{CDOM}(\lambda) = (2.303/l) \times ((OD_{CDOM}(\lambda) - OD_{Milli-Q}(\lambda)) - OD_{null}), \quad (1)$$

where $OD_{CDOM}(\lambda)$ and $OD_{Milli\text{-}Q}(\lambda)$ are respectively measured the light absorbance of CDOM sample and purified Milli-Q water at wavelength λ; l denotes the quartz cell path length (0.1 m); OD_{null} is the residual absorbance offset at the long wavelength, average value of (OD_{CDOM}-$OD_{Milli\text{-}Q}$) from 695 to 705 nm was used. Some examples of CDOM absorption coefficient spectra for different salinities are shown in Fig. 2a. With known a_{CDOM}(400), the absorption coefficient at any wavelength λ ($a_{CDOM}(\lambda)$) can be calculated using the embedded equation, with S_{CDOM} of the spectral slope (Fig. 2a).

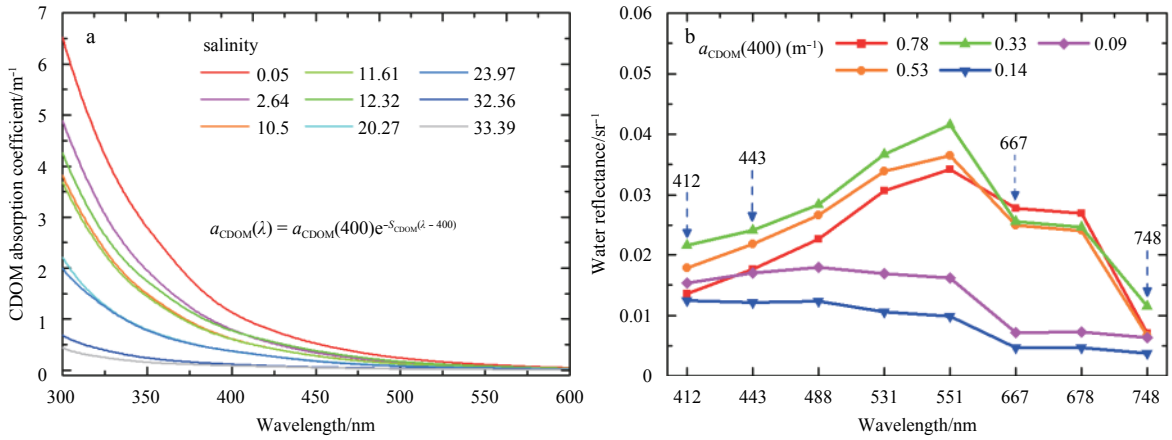

Fig. 2. Examples of *in situ* measurements in the RRE. a. CDOM absorption spectra for waters with different salinities. S_{CDOM} is the CDOM spectral slope; and b. equivalent water reflectance spectra with different a_{CDOM}(400). 412, 443, 667, 748 nm are commonly used wavelengths for ocean color remote sensing. Equivalent water reflectance spectrum was calculated using Eq. (3).

DOC samples were also collected following the protocols established by the joint global ocean flux study (JGOFS) (Knap et al., 1994). The DOC samples were measured via a high temperature combustion method (680°C) using a total organic analyzer (Shimadzu, Inc) by referring to standard seawater samples provided by the Hansell Laboratory, Miami University. For a specific DOC sample, an analytic precision was within 2% on triplicate injections (Liu et al., 2014). More details about collection, storage, and measurement of DOC samples can be found in Liu et al. (2014).

3.1.2 *Water reflectance*

When collecting water, the radiances of water surface (L_{ws}), sky light (L_{sky}), and a standard reflecting plate (L_p) were also measured by a field Spec spectroradiometer (Analytical Spectral Devices Inc,) using the above-water method following the ocean optics protocols proposed by the NASA (Mueller et al., 2003; Bai

et al., 2013; Liu et al., 2015). Before the cruises, absolute calibration was performed to the instrument using an NIST traceable lamp in the laboratory (He et al., 2013). When measuring L_{ws} and L_{sky}, the probe was positioned at an angle of 90°–135° to the plane of an incident radiation so as to minimize the effects of sun glint and ship shadow (Liu et al., 2015). A view angle to the aplomb direction was 135°–150° for L_{ws}, but 30°–45° for L_{sky}. After measuring L_{ws} and L_{sky}, L_p was collected similar to L_{ws} but with probe vertical to the standard reflecting plate. The Field Spec Spectroradiometer recorded L_{ws}, L_{sky} and L_p ranging from 350 nm to 2 390 nm with an interval of 1 nm. Then, water reflectance (R_{rs}) was calculated as follows:

$$R_{rs}(\lambda) = \rho(\lambda)(L_{ws}(\lambda) - rL_{sky}(\lambda))/(\pi L_p(\lambda)), \quad (2)$$

where for a specific wavelength λ, $R_{rs}(\lambda)$ is the water reflectance; $\rho(\lambda)$ is the reflectance of the standard reflecting plate; $L_{ws}(\lambda)$, $L_{sky}(\lambda)$ and $L_p(\lambda)$ are the radiance of water surface, sky light, and the standard reflecting plate respectively; r is the reflectance of air-water interface, with r=0.28 for the waters in the ZJE (Liu et al., 2015).

For a specific band of MODIS/Aqua, it majorly received radiance within a ZJE viously designed band range. To develop CDOM algorithms applicable to MODIS/Aqua data, equivalent water reflectance (r_{equi}, sr^{-1}) for its ocean color bands of the *in situ* water reflectance was computed firstly. For a specific band, r_{equi} was calculated using Eq. (2) (Liu et al., 2015).

$$r_{equi}(\lambda) = \frac{\int_{350}^{800} f(\lambda)R_{rs}(\lambda)I(\lambda)\mathrm{d}\lambda}{\int_{350}^{800} f(\lambda)I(\lambda)\mathrm{d}\lambda}, \quad (3)$$

where λ (412, 443, 488, 531, 551, 667, 678 or 748 nm) is the central wavelength representing the specific band. For band λ, $f(\lambda)$ is the spectral response function from the OceanColor Website (http://oceancolor.gsfc.nasa.gov/); $L(\lambda)$ is the solar irradiance at the mean earth-sun distance. For band λ of MODIS/Aqua, $f(\lambda)$ is close to 0 beyond 350–800 nm, so we set the integration range of 350–800 nm.

3.1.3 *Others*

A SBE 19 plus CTD (Sea-Bird Electronics, Inc., USA) was used to record profile parameters at a frequency of 6 Hz. For a specific station, surface salinity was calculated by averaging CTD records within 0.5 m depth. In the summer cruise, the seapoint ultraviolet fluorometer was employed to record underway CDOM fluorescence, with an excitation wavelength of 370 nm and emission wavelength of 440 nm.

3.2 *Satellite data*

Daily level 1 B calibrated radiance products of MODIS/Aqua (MYD021KM, Version 2.16) were downloaded from the Level 1 and atmosphere archive and distribution system (http://ladsweb.nascom.nasa.gov/). Level 1 B data of MODIS/Aqua in January, April, July and November were downloaded from 2002 to 2014. All MODIS/Aqua data scanned the ZJE at about 1:30 pm local time with spatial resolution at the nadir point of 1 000 m×1 000 m for ocean color bands. On the basis of the SeaWiFS data analysis system (SeaDAS, Version 6.4), a near-infrared and shortwave infrared bands atmospheric correction algorithm was applied to MYD021KM to remove atmospheric effects and retrieve the water reflectance. When processing the MODIS/Aqua Level 1 B data, the L2 processing flags set by the atmospheric correction algorithm was used to identify and exclude questionable pixels, such as pixels of land, cloud, sun glint, etc. (Bailey and Werdell, 2006). Pixel with the reflectance of band centered at 2 030 nm larger than 0.018 was labeled as cloud. The atmospheric correction algorithm can derive the water reflectance of clearly open sea as well as turbid estuary from MODIS/Aqua Level 1 B data (Wang and Shi, 2007). Finally, the output reflectance data with precisely geographic coordinate was clipped for studying the ZJE (Fig. 1).

4 Remote sensing algorithms

4.1 *CDOM*

As one of ocean color products, CDOM was often derived from optical satellite data (Siegel et al., 2002; Belanger et al., 2008; Mannino et al., 2008). Most previous CDOM algorithms were based on band ratios which could enhance CDOM signal and weaken effect of atmospheric correction error (Chen et al., 2003; Fang et al., 2009; Siswanto et al., 2011). However, algorithms for open oceans or other estuarine waters may not be suitable for intensively varied waters in the ZJE (Sections 1 and 2), of which two broad classes were identified: one was with high CDOM concentration and water reflectance, but the other one was opposite (Fig. 2). For the ZJE, temperature and discharge from the Zhujiang River are high in summer, but on the contrary in winter (Section 2). Spring and autumn are the two transitional seasons. Therefore, the CDOM data (Section 3.1) and equivalent water reflectance (Eq. (3)) from winter and summer cruises, 45 in all, were applied to develop and parameterize the CDOM algorithm. In this case, the developed algorithm can be used to all seasons.

For the ZJE, $a_{CDOM}(400)$ was positively linearly related to TSM concentration (R^2=0.28, P<0.05). Suspended particle can significantly scatter light and increase the water reflectance at the long wavelength. Both water reflectance at 667 nm ($R_{rs}(667)$) and 748 nm ($R_{rs}(748)$) were positively linearly correlated with the TSM concentration, with R^2=0.52 for $R_{rs}(667)$ (P<0.05) and R^2=0.17 for $R_{rs}(748)$ (P<0.05). Moreover, strong CDOM light absorption at 412 nm and 443 nm could decease the water reflectance $R_{rs}(667)$ and ($R_{rs}(748)$) (Fig. 2a). Therefore, both ratios of $R_{rs}(667)$ to $R_{rs}(443)$ and $R_{rs}(748)$ to $R_{rs}(412)$ can denote the CDOM concentration in the ZJE. To inverse CDOM concentration in the ZJE, in fact, Chen et al. (2003) and Fang et al. (2009) previously used ratios of $R_{rs}(670)$ to $R_{rs}(412)$ and $R_{rs}(703)$ to $R_{rs}(488)$, respectively. After testing various band combinations, the CDOM algorithm that was applicable to intensely dynamic waters in the ZJE was shaped and parameterized as follows (Fig. 3).

$$a_{CDOM}(400) = 0.158\ 1\left(\frac{r_{equi}(667)}{r_{equi}(443)}\right)^{1.626\ 7}\left(\frac{r_{equi}(784)}{r_{equi}(412)}\right)^{-0.981\ 7}, \quad N = 45,\ \ R^2 = 0.923\ 0, \quad (4)$$

where $a_{CDOM}(400)$ denotes CDOM absorption coefficient at 400 nm; $r_{equi}(667)$, $r_{equi}(443)$, $r_{equi}(748)$ and $r_{equi}(412)$ were defined as Eq. (3). With R^2=0.923 0, the used wavelengths can reflect different sources of CDOM in the ZJE (Eq. (4)). Arenz et al. (1996) reported a similar algorithm to inverse the DOC concentration in eight reservoirs of the Colorado Front Range. The detailed process was shown in Fig. 3.

Moreover, an absolute error (*AE*), a relative error (*RE*), and a

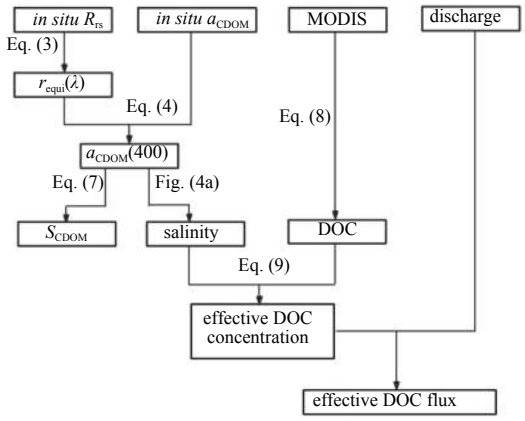

Fig. 3. Flowchart of the developed algorithms. Discharge was the annual discharge of the Zhujiang River from the Ministry of Water Resources of the People's Republic of China (MWR, http://www.mwr.gov.cn).

mean square error (*RMSE*) were employed to evaluate the modeling results. They are defined by referring to Świrgoń and Stramska (2015) as follows:

$$\left.\begin{aligned} AE &= V_{\text{modeled}} - V_{in\ situ} \\ RE &= (V_{\text{modeled}} - V_{in\ situ})/V_{in\ situ} \times 100\% \\ RMSE &= \sqrt{\sum_{i=1}^{N}(V_{in\ situ} - V_{\text{modeled}})^2/(N-1)} \end{aligned}\right\}, \quad (5)$$

where V_{modeled} denotes the modeled value; $V_{in\ situ}$ represents the *in situ* value; and N is the sample size.

4.2 *CDOM spectral slope*

Waters with same $a_{CDOM}(400)$ may vary in composition due to different sources. Optical properties can be used to explore the CDOM composition (Chen et al., 2004). The spectral slope is the fitting slope of the CDOM absorption coefficient (Fig. 2a). S_{CDOM} has been successfully applied to indicate sources and transformation processes of CDOM (Jaffé et al., 2004). During the cruises, the *in situ* S_{CDOM} varied between 0.010 7 nm^{-1} and 0.017 6 nm^{-1}, which were consistent with the observations of Hong et al. (2005). For the Gulf of Mexico, Carder et al. (1989) calculated the spectral slope using a spectral range of 370–440 nm. In order to compare with their results, we also calculated S_{CDOM} over the same spectral range. S_{CDOM} was deduced from the CDOM absorption equation (Fig. 2a) and shaped as as follows (Fig. 3).

$$S_{CDOM} = \frac{\ln(a_{CDOM}(370)/a_{CDOM}(440))}{70}, \quad (6)$$

where $a_{CDOM}(370)$ and $a_{CDOM}(440)$ are the CDOM absorption coefficient at 370 nm and 440 nm, respectively. For all *in situ* data, $a_{CDOM}(370)$ and $a_{CDOM}(440)$ were greatly linearly related to $a_{CDOM}(400)$, with R^2 of 0.995 8 and 0.992 7, respectively. From the CDOM absorption equation embedded in the Fig. 2a, moreover, both $a_{CDOM}(370)$ and $a_{CDOM}(440)$ can be inversed using a similar satellite algorithm as $a_{CDOM}(400)$. Using the *in situ* data from four conducted cruises in the ZJE (57 in all), Eq. (6) was parameterized, with *RMSE* of 0.837 9 nm^{-1} and mean absolute RE of 4.364 7%. The parameterized S_{CDOM} algorithm is shown as follows:

$$S_{CDOM} \times 1\,000 = 14.235 + 3.0558 \ln\left(\frac{r_{equi}(667)}{r_{equi}(443)}\right) - 1.1843 \ln\left(\frac{r_{equi}(748)}{r_{equi}(412)}\right), \quad N = 57,\ R^2 = 0.779\ 1, \quad (7)$$

where $r_{equi}(667)$, $r_{equi}(443)$, $r_{equi}(748)$ and $r_{equi}(412)$ were defined as Eq. (3).

4.3 *Effective riverine end-member DOC*

CDOM was usually conservatively mixed in estuaries (Pan et al., 2012). Hong et al. (2005) reported that CDOM was conservatively mixed in the ZJE. Our *in situ* data also evidenced the conservative mixing by a negatively linear relation between $a_{CDOM}(400)$ and salinity (Fig. 4a). For DOC, Dai et al. (2000) reported that DOC concentration followed a mixing line beyond salinity 5 until 25 in winter (March 1997) in the ZJE. The conservative mixing was disturbed by DOC from transformations of particulate organic carbon in low salinity waters (Dai et al., 2000) or DOC produc-

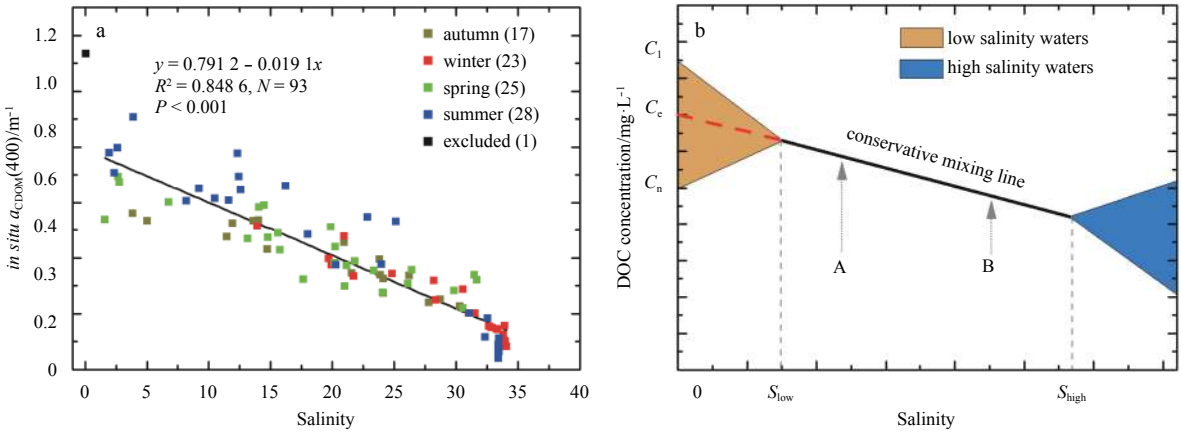

Fig. 4. DOM (the CDOM and the DOC) mixing in the ZJE. a. Conservative mixing of CDOM. The embedded equation was parameterized using *in situ* data with salinity larger than 1.5 from four conducted cruises; b. DOC mixing diagram. DOC in waters with salinities lower than S_{low} and higher than S_{high} are not conservatively mixed. Regions A and B are defined as in Fig. 1b. C_1, C_2, ..., and C_n are DOC concentrations at different outlets of the Zhujiang River.

tion by phytoplankton in high salinity waters. Figure 4 shows DOM mixing diagram in the ZJE. Supposing DOC is conservatively mixed in waters with salinity from S_{low} to S_{high} (Fig. 4b), effective riverine end-member DOC concentration (C_e) can be calculated using the DOC conservative mixing line (Fig. 4b). However, DOC mixing in estuary was often not conservative and seasonally varied (Pan et al., 2012). For the four conducted cruises, conservative DOC mixing was only significant for waters in summer with salinities larger than 1.5 (R^2=0.798 and N=28) and winter with salinities larger than 10 (R^2=0.789 8 and N=27). Therefore, only seasonal C_e in summer and winter was estimated in this study.

For a specific time, using the CDOM mixing equation (Fig. 4a) and the developed CDOM algorithm (Eq. (4)), the salinities in Regions A (S_A) and B (S_B) were calculated (Fig. 1b). Furthermore, Chen et al. (2003) reported a remote sensing algorithm to inverse the DOC concentration in the ZJE. Using all *in situ* data from four conducted cruises in the ZJE (Section 3.1), their DOC algorithm was parameterized, with RMSE 0.156 6 mg/L of and mean absolute RE of 10.452 7%. The parameterized equation is shown as Eq. (8):

$$\begin{aligned} \ln[\mathrm{DOC}] = {} & 0.265\ 9 \times \ln \frac{r_{equi}(667)}{r_{equi}(412)} + 0.248\ 8, \\ N = {} & 57, R^2 = 0.490\ 8, \end{aligned} \tag{8}$$

where $r_{equi}(667)$ and $r_{equi}(412)$ are defined as in Eq. (3). Using Eq. (8), the DOC concentrations in Regions A (DOC_A) and B (DOC_B) were calculated. On the basis of the above estimated salinities and DOC concentrations in Regions A and B, the conservative mixing line of DOC in Fig. 4b was parameterized and applied to compute C_e shown as follows:

$$C_e = ((DOC_A - DOC_B) \times S_A)/(S_B - S_A) + DOC_A. \tag{9}$$

Finally, effective riverine end-member DOC flux (F_e) was also calculated by multiplying C_e by discharge of the Zhujiang River. The detailed processes are shown in Fig. 3.

5 Results

5.1 *CDOM algorithm validation*

5.1.1 *Comparing with in situ $a_{CDOM}(400)$*

The *in situ* data from autumn cruise (12 in total) was used to validate the reliability of the developed CDOM algorithm (Eq. (4)). Figure 5 shows the validation results of modeled $a_{CDOM}(400)$ based on the *in situ* $a_{CDOM}(400)$. For all the 57 *in situ* data, RMSE, mean absolute AE (|AE|), and mean absolute RE (|RE|) of modeled $a_{CDOM}(400)$ were 0.073 6 m^{-1}, 0.052 1 m^{-1}, and 15.874 4%, respectively (Fig. 5). For the 12 testing data alone, *RMSE*, mean |*AE*|, and mean |RE| were 0.062 7 m^{-1}, 0.048 2 m^{-1}, and 12.428 7%, respectively. Application results of the new developed algorithm to *in situ* the water reflectance were satisfactory. Using the developed algorithm, the CDOM concentration in the ZJE can be inversed from the water reflectance.

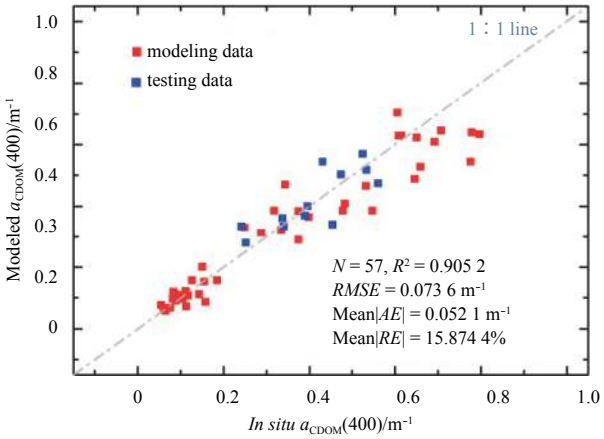

Fig. 5. Comparisons between *in situ* $a_{CDOM}(400)$ and modeled $a_{CDOM}(400)$ calculated from the *in situ* water reflectance using the developed CDOM algorithm (Eq. (4)). The water reflectance was no available in the spring cruise.

5.1.2 *Comparing with other algorithms*

Furthermore, the developed CDOM algorithm was compared with other three algorithms which had been developed to inverse coastal CDOM concentration (Table 1). All the four algorithms got preferable modeling results for waters with $a_{CDOM}(400)$ around 0.35 m^{-1}. For waters with $a_{CDOM}(400)$ higher than 0.6 m^{-1}, however, algorithm proposed by Dong et al. (2013) significantly overestimated $a_{CDOM}(400)$, but for other three algorithms (Fig. 6). For waters with $a_{CDOM}(400)$ lower than 0.3 m^{-1}, on the contrary, algorithm proposed by Dong et al. (2013) significantly underestimated $a_{CDOM}(400)$, but for other three algorithms (Fig. 6).

For algorithms proposed by D'sa and Miller (2003) and Tiwari and Shanmugam (2011), modeling results were similar for waters with high $a_{CDOM}(400)$, but the latter one got greater *RE* for waters with $a_{CDOM}(400)$ lower than 0.3 m^{-1}, with unexpectedly great *RE* of 264.94% (Fig. 6). Water environment in the ZJE was locally characterized, with high TSM concentration (Ni et al., 2008) and $a_{CDOM}(400)$. When water was turbid, Zhu et al. (2011) previously reported that the accuracy of QAA algorithm generally degraded rapidly with increasing CDOM and non-algal particle concentrations. With poor regional and seasonal knowledge of inherent optical properties in the ZJE, the QAA algorithm also did not perform well in the ZJE (Fig. 6). With least |RE| (15.87%), in general, the new developed algorithm (Eq. (4))

Table 1. Other three coastal CDOM algorithms developed by D'sa and Miller (2003), Tiwari and Shanmugam (2011) and Dong et al. (2013). The former two were parameterized using all the 57 *in situ* data from cruises in the ZJE (Section 3.1). $r_{equi}(670)$, $r_{equi}(412)$, $r_{equi}(510)$, $r_{equi}(555)$ and $r_{equi}(490)$ were calculated using Eq. (3)

Algorithm	Best-fitted relationships	|*RMSE*|/m^{-1}	Mean |*RE*|/%
D'sa and Miller (2003)	$\ln(a_{CDOM}(400)) = -1.552\ 3 - 2.531\ 4 \times \ln\left(\frac{r_{equi}(510)}{r_{equi}(555)}\right)$	0.158 5	35.13
Tiwari and Shanmugam (2011)	$a_{CDOM}(400) = -0.001\ 4 + 0.552 \times \frac{r_{equi}(670)}{r_{equi}(490)}$	0.162 8	59.66
Dong et al. (2013)	QAA algorithm	0.264 0	54.83

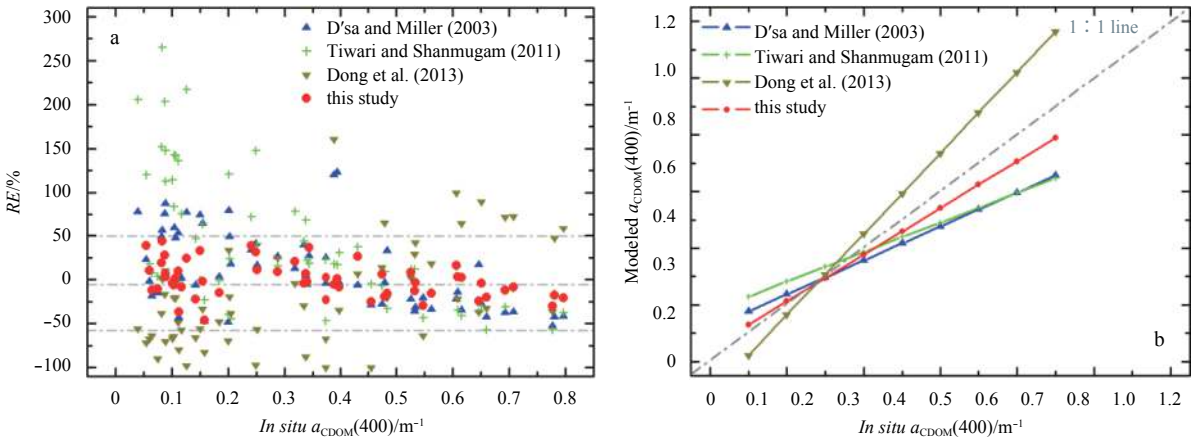

Fig. 6. Comparing with other three CDOM algorithms (Table 1). a. Relative error (Eq. (5)) and b. regression lines between *in situ* $a_{CDOM}(400)$ and modeled $a_{CDOM}(400)$ using different algorithms.

was better than other three algorithms (Fig. 6a). The developed algorithm was more applicable to the highly turbid waters in the ZJE.

5.1.3 *Application to MODIS/Aqua data*

The developed algorithm was applied to the satellite water reflectance of MODIS/Aqua so as to further validate its availability (Section 3.2). When matching *in situ* measurement and satellite observation, we set the space window as 3×3 pixels so as to account for possible navigation error for the tempo-spatially dynamic waters in the ZJE (Bailey and Werdell, 2006). In order to allow for a greatest match possibility, the time window was set as ±3 h (Bailey and Werdell, 2006; He et al., 2013). To do the matching up for the coastal waters in the ZJE, mean value was calculated only for sampled stations with a minimum of five valid pixels. With the space window of 3×3 pixels and time window of ±3 h, only six stations were found. The AE and RE of satellite-derived $a_{CDOM}(400)$ are shown in Table 2. For $a_{CDOM}(400)$, mean |AE| was 0.067 m^{-1}, with minimum of 0.000 4 m^{-1} and maximum of 0.200 3 m^{-1}; mean |RE| was 18.127%, with minimum of 0.507 5% and maximum of 44.773 8% (Table 2). In general, the application results were acceptable.

Moreover, an underway CDOM concentration was also used to evaluate application of the developed algorithm to MODIS/Aqua data. Underway $a_{CDOM}(400)$ was computed from recorded CDOM fluorescence (QSU) through the fitted linear equation

Table 2. Application results of the developed CDOM algorithm to MODIS/Aqua data. AE and RE were defined as Eq. (5)

No.	Local time	*In situ* $a_{CDOM}(400)/m^{-1}$	Satellite-derived $a_{CDOM}(400)/m^{-1}$	$\|AE\|/m^{-1}$	$\|RE\|/\%$
1	2014-02-27 11:15	0.088	0.087 6	0.000 4	0.507 5
2	2014-02-27 12:00	0.082	0.083 6	0.001 6	1.999 8
3	2014-02-27 14:04	0.158	0.087 3	0.070 7	44.773 8
4	2014-02-27 14:55	0.101	0.091 9	0.009 1	9.044 7
5	2014-08-24 15:14	0.616	0.495 6	0.120 4	19.538 4
6	2014-08-24 16:23	0.609	0.408 7	0.200 3	32.898

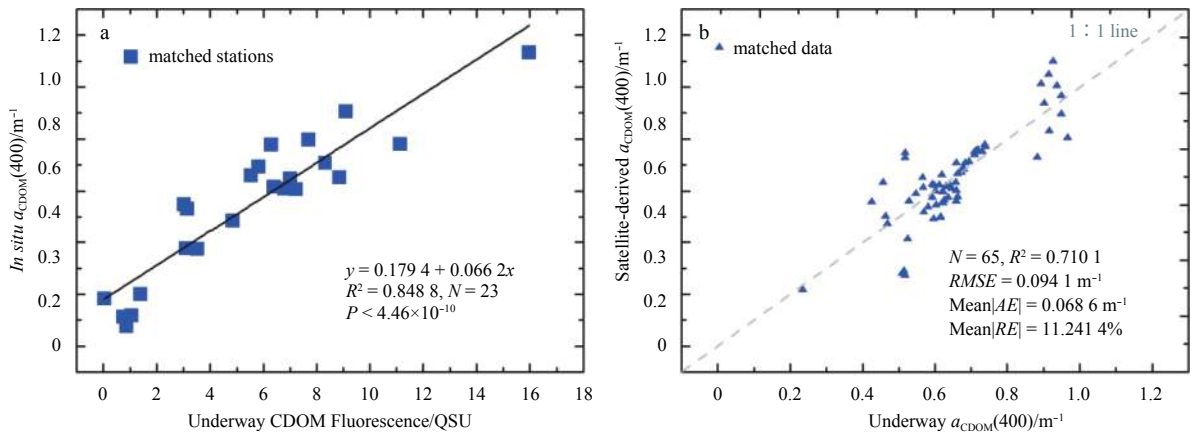

Fig. 7. Validating the new developed CDOM algorithm using underway $a_{CDOM}(400)$ from summer cruise. a. The linear correlation between the *in situ* $a_{CDOM}(400)$ and the underway CDOM fluorescence; and b. validation result of satellite-derived $a_{CDOM}(400)$ based on underway $a_{CDOM}(400)$ calculated from the CDOM fluorescence.

embedded in Fig. 7a. When matching underway measurement and satellite observation, similar screening rules as the *in situ* measurement were adopted. However, the mean value of underway $a_{CDOM}(400)$ 1 km around the central pixel of the 3×3 pixels array was calculated . For the 65 matched underway $a_{CDOM}(400)$, validation results were also desirable, with RMSE of 0.094 1 m^{-1}, mean |AE| of 0.068 6 m^{-1}, and mean |RE| of 11.241 4% respectively (Fig. 7b). In sum, based on the MODIS/Aqua data and the Eq. (4), distributions and dynamics of CDOM in the ZJE can be monitored in high tempo-spatial resolution from space.

5.2 *Tempo-spatial variations of CDOM*

Table 3 shows the statistical results of *in situ* $a_{CDOM}(400)$ from four seasonal cruises. $a_{CDOM}(400)$ was negatively linearly related to salinity (Fig. 4a). With different salinities, $a_{CDOM}(400)$ changed with sampling sites (Fig. 1b). Discharge from the Zhujiang River was lowest in winter, with minimum *in situ* salinity of 13.904 and mean $a_{CDOM}(400)$ of only 0.212 m^{-1}. When with the highest discharge in summer, the minimum *in situ* salinity and mean $a_{CDOM}(400)$ were 0.047 m^{-1} and 0.448 m^{-1}, respectively. Moreover, *in situ* $a_{CDOM}(400)$ were similar in autumn and spring when with similar discharges (Table 3). In short, *in situ* $a_{CDOM}(400)$ presented greatly tempo-spatial variations in the ZJE.

Equation (4) was applied on daily satellite water reflectance to calculate daily $a_{CDOM}(400)$ from 2002 to 2014 (Section 3.2). Then, monthly satellite climatology $a_{CDOM}(400)$ was calculated by averaging daily $a_{CDOM}(400)$ of a specific month. The results are shown as Fig. 8. Agreeing with the *in situ* data (Table 3), satellite-derived seasonal $a_{CDOM}(400)$ intensely varied with season and space. For the same area, $a_{CDOM}(400)$ in summer was significantly higher than those in other seasons, especially for near shore waters (Fig. 8). Surface area percent of waters with $a_{CDOM}(400)$ ranging from 0 to 1 m^{-1} (with interval of 0.1 m^{-1}) is shown in Fig. 9a. $a_{CDOM}(400)$ in most areas was lower than 0.3 m^{-1}, with maximum area percent of 28.73% from 0.1 to 0.2 m^{-1} in autumn, 50.37% in winter, 60.94% in spring and 27.77% in summer but from 0.2 to 0.3 m^{-1} (Figs 8 and 9a). The area percent of waters with seasonal $a_{CDOM}(400)$ higher than 0.3 m^{-1} was 42.66% in autumn, 24.16% in winter, 16.90% in spring and 43.49% in summer, respectively (Fig. 8).

In terms of space, satellite-derived seasonal $a_{CDOM}(400)$ was low for off shore waters with high salinities (Fig. 8). Along Section P (Fig. 1b), seasonal $a_{CDOM}(400)$ was intertwined in near shore waters, with the maximum in summer and minimum in spring; seasonal $a_{CDOM}(400)$ was close to each other in off shore waters east of 114.0°E (Fig. 9b). The Lingding Bay was the major mixing zone of riverine and saline waters. Seasonal $a_{CDOM}(400)$ was higher in the west part of the Lingding Bay, especially in spring and summer when with higher discharge from the Zhujiang River (Table 3, Fig. 8). However, this distribution pattern was not very obvious in winter and autumn when with low discharge. In the north-south direction, seasonal $a_{CDOM}(400)$ was higher in the Lingding Bay than that in the south of 22°N. In the south of 22°N, most high values of seasonal $a_{CDOM}(400)$ happened in the west near shore waters which were mixed by fresh water from the Zhujiang River (see Figs 1 and 8). Along Section P (Fig. 1b), seasonal $a_{CDOM}(400)$ exponentially decreased from near shore to off shore waters with increasing longitude and salinity (Fig. 8). Moreover, decreases of seasonal $a_{CDOM}(400)$ in all seasons could be fitted with exponential equations ($y=ae^{bx}$, $b<0$), with R^2 of 0.943 1 in autumn, 0.923 1 in winter, 0.753 8 in spring, and 0.971 4 in summer, respectively.

5.3 *The effective DOC flux into the SCS by the Zhujiang River*

Waters in Regions A and B were with different salinities (Fig. 1b). On the basis of the developed CDOM algorithm (Eq. (4)) and the CDOM conservative mixing equation (Fig. 4a), not only the mean $a_{CDOM}(400)$ in Regions A and B were estimated

Table 3. Descriptive statistics of *in situ* $a_{CDOM}(400)$ in the ZJE. More details were described in the Section 3.1.1. Discharge calculation covered the sampling month and two months before.

Cruise (samples)	Discharge/10^8 m^3	Salinity	$a_{CDOM}(400)/m^{-1}$	Mean $a_{CDOM}(400)/m^{-1}$	Median $a_{CDOM}(400)/m^{-1}$
Autumn (18)	559.635	3.83–30.28	0.227–0.562	0.399	0.392
Winter (27)	336.617	13.904–34.066	0.082–0.515	0.212	0.155
Spring (29)	874.919	1.6–31.7	0.219–0.694	0.423	0.389
Summer (29)	1229.659	0.047–33.628	0.04–1.134	0.448	0.532
All (103)	–	0.047–34.066	0.04–1.134	0.371	0.355

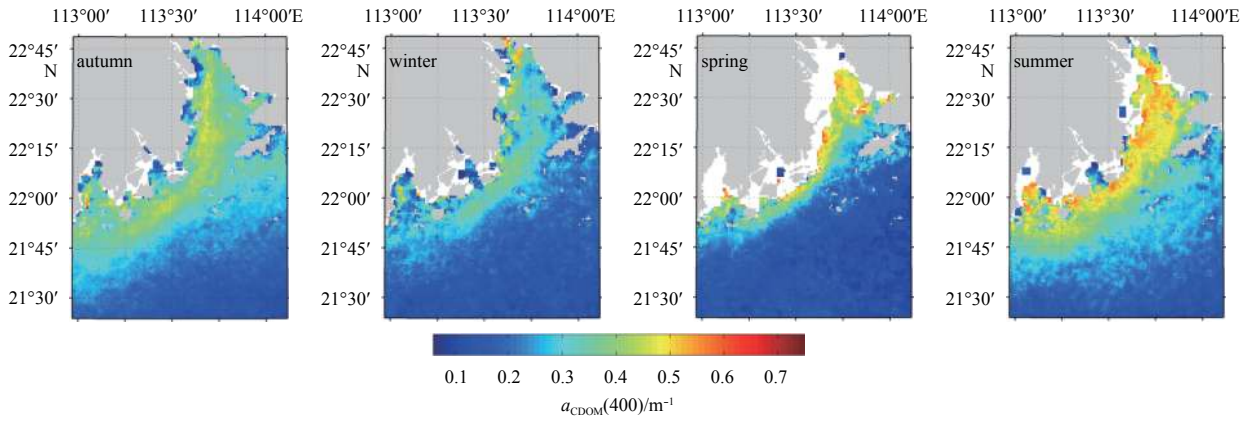

Fig. 8. Satellite-derived seasonal $a_{CDOM}(400)$ in the ZJE. Seasonal $a_{CDOM}(400)$ was denoted by the mean value in a specific month from 2002 to 2014, with November for autumn, January for winter, April for spring, and July for summer. Owing to light influence from land objects, few values near the land were abnormal.

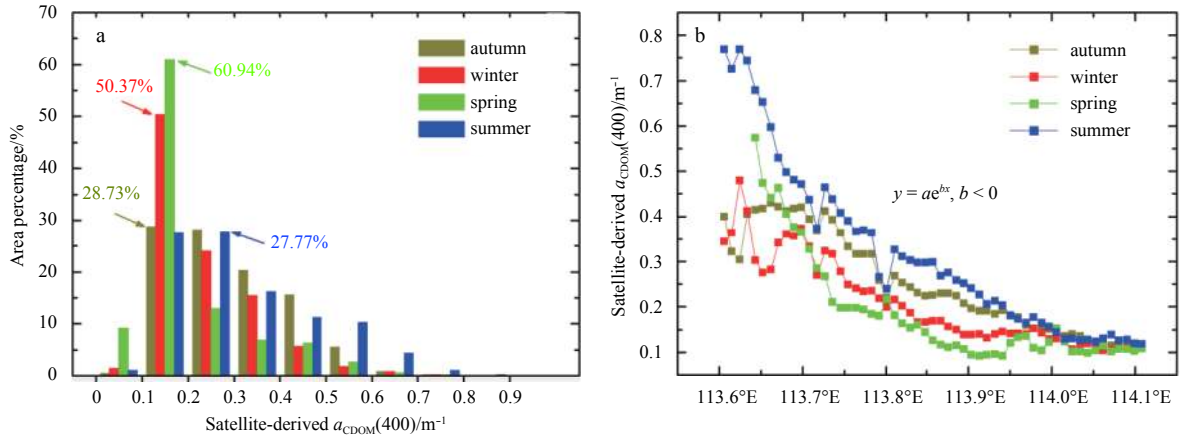

Fig. 9. Tempo-spatial variations of seasonal $a_{CDOM}(400)$ in the ZJE. a. Frequency histogram of seasonal $a_{CDOM}(400)$ in different seasons; and b. seasonal $a_{CDOM}(400)$ along the Section P in different seasons (Fig. 1b). The Wanshan Islands are located around 113.8°E.

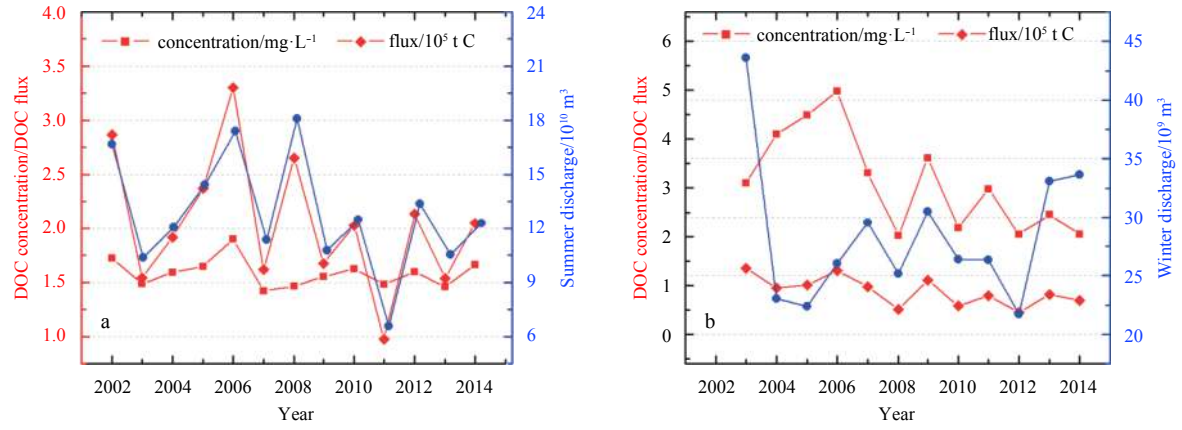

Fig. 10. Effective riverine end-member DOC concentration and flux into the SCS in summer (a) and winter (b) from 2002 to 2014. For a specific year, summer includes June, July and August; winter contains January, February and December of the year before. Discharge is the sum of monthly discharges measured at the Boluo, Shijiao and Gaoyao Hydrometric Stations.

from the MODIS/Aqua data, but also the mean salinities. Using Eq. (8), mean DOC concentrations in Regions A and B were also calculated from the MODIS/Aqua data. Following the calculation processes (Fig. 3), effective riverine end-member DOC concentrations and fluxes in winter and summer from 2002 to 2014 were calculated (Fig. 10).

In summer from 2002 to 2014, mean C_e was 1.59 mg/L, with minimum of 1.42 mg/L in 2007 and maximum of 1.9 mg/L in 2006. Mean F_e was 2.05×10^5 t, with minimum of 0.98×10^5 t in 2011 and maximum 3.3×10^5 of in 2006 (Fig. 10a). In summer, C_e was positively linearly related to discharge (R^2=0.698) except for 2008, when riverine DOC concentration might be diluted by discharge as high as 18.09×10^{10} m^3. It was the same to F_e, with R^2 of 0.965 7 (Fig. 10a). In winter except for 2004, 2005 and 2006, mean C_e was 2.64 mg/L, with minimum of 2.02 mg/L in 2008 and maximum of 3.62 mg/L in 2009. Mean F_e was 0.81×10^5 t, with minimum of 0.46×10^5 t in 2012 and maximum of 1.35×10^5 t in 2003 (Fig. 10b). Except for 2004–2006, C_e and F_e were also positively related to discharge in winter, but more weakly than those in summer. With low water discharge of the Zhujiang River from 2004 to 2006, photosynthetic active radiation in Region A might increase (Section 1). Part DOC in Region A might be produced by *in situ* phytoplankton. As results, the values of C_e in these years might be overestimated.

6 Discussion

6.1 *Sources and spectral slope of CDOM*

First, massively terrigenous CDOM was discharged into estuary along with riverine fresh water (Ni et al., 2008; Wang et al., 2012). The greatly linear relationship between $a_{CDOM}(400)$ and the salinity (Fig. 4a) indicated the great contribution of terrigenous CDOM in the ZJE (Hong et al., 2005). Secondly, terrestrial nutrient loadings could fuel a high phytoplankton production in estuarine regions (Callahan et al., 2004); and phytoplankton degradation could further produce CDOM. However, there was no correlation between *in situ* $a_{CDOM}(400)$ and Chl *a*, so the CDOM contribution by phytoplankton should be limited in the ZJE. Thirdly, microbial community can produce CDOM by transforming non-colored DOM to CDOM. The high fluorescence signature of low salinity waters in the ZJE, reported by Callahan et al. (2004), might be attributed to microbial transformation of non-fluorescent DOM to fluorescent CDOM. In addition, marsh and wetland within the estuarine system can also produce CDOM. However, with little marsh and wetland in the highly engineered estuary, CDOM from these sources was assumed to be small in

the ZJE (Callahan et al., 2004). Judging from the conservative mixing (Fig. 4a), CDOM sourced from phytoplankton, microbial communities, and wetlands, etc, just balanced degradation of riverine CDOM; and fresh water was the primary source of CDOM in the ZJE.

Equation (7) was applied to the daily satellite water reflectance of MODIS/Aqua to calculate daily S_{CDOM} from 2002 to 2014 (Section 4.2). Then, monthly satellite climatology S_{CDOM} was calculated by averaging daily S_{CDOM} of a specific month. The results are shown as Fig. 11. S_{CDOM} was reported negative correlation with the CDOM concentration in coastal waters of the Bohai Sea (Xing et al., (2008) and references therein). However, it was not the case in the ZJE, where S_{CDOM} decreased significantly along Section P with decreasing $a_{CDOM}(400)$ (Figs 1b, 9b and 11). There was a positive correlation between S_{CDOM} and $a_{CDOM}(400)$ in the ZJE, with R^2=0.689 2. Fulvic acid and humic acid are the primary components of CDOM. The spectral slope of fulvic acid was higher than that of humic acid (Carder et al., 1989). Therefore, S_{CDOM} can serve as an indicator for the fulvic acid fraction of CDOM (Carder et al., 1989). For the Mississippi Plume, Carder et al. (1989) reported a logarithmic relation between S_{CDOM} and the fulvic acid fraction ([fulvic acid fraction]=$a$ln(S_{CDOM})+b). For the ZJE, fulvic acid fraction decreased with decreasing S_{CDOM} and increasing salinity in both winter and summer (Fig. 11). S_{CDOM} and fulvic acid fraction were high in near shore waters with low salinities. It might be due to high fulvic acid fraction of terrigeous CDOM, flushed from soils with richly fulvic acid (Yu and Bai, 1962). For the near shore waters in winter and summer, the great discrepancy of fulvic acid fraction might be attributed to the fact that more fulvic acid was degraded with the longer residence time in winter (Sun et al., 2014). The remaining CDOM was persistent, so the fulvic acid fraction decreased slightly in the waters with high salinities (Fig. 10).

6.2 *Factors influencing CDOM distribution in the ZJE*

Many physical-biogeochemical processes, such as water advection, photo-bleaching, bacterial utilization (Amon and Benner, 1996; Hong et al., 2005), phytoplankton growth, etc., can impact the CDOM distribution in estuarine waters. CDOM was majorly sourced from fresh water and was conservatively mixed in the ZJE (Fig. 4a). Moreover, before entering into the SCS, the average residence time of fresh water in the Lingding Bay was short, with about 6 days during the dry season and 3 days in the wet season (Sun et al., 2014). Therefore, river discharge and factors that influence the fresh water diffusion should be the major impact factors on the CDOM distribution in the ZJE.

The discharge of the Zhujiang River, high in summer (wet season) and low in winter (dry season) (Callahan et al., 2004; Chen et al., 2004; Liu et al., 2015), has significant influence on the distribution pattern of $a_{CDOM}(400)$ in the ZJE (Section 5.2). With low discharge and strongly northeast wind during the dry season, the Zhujiang River plume is advected westward by Guangdong coastal current and tidal flood current. Small area with $a_{CDOM}(400)$ higher than 0.3 m^{-1} (Figs 8 and 9b) was synchronous with the much small plume area in winter (Dong et al., 2004). At high discharge, however, fresh water could diffuse far away. For the peak discharge season of the Changjiang River, the plume area was greatly positively correlated with the water discharge (Bai et al., 2014). With high discharge and eastward Guangdong coastal current under strongly southwest wind, the Zhujiang River plume could intrude eastward even into the Penghu Channel during the wet season (Dong et al., 2004; Bai et al., 2015). The area of low salinity waters with $a_{CDOM}(400)$ larger than 0.3 m^{-1} in summer (high discharge season) was apparently larger than that in winter (Figs 8 and 9b). Moreover, there was a significantly positive correlation between the discharge of the Zhujiang River and the area percent of waters with high $a_{CDOM}(400)$ in the ZJE, especially for waters with $a_{CDOM}(400)$ larger than 0.25 m^{-1} in summer (Fig. 12). However, due to strongly vertical mixing, low discharge from the Zhujiang River, and long residence in winter, no obvious relation among them was found.

Besides river discharge, an estuarine underwater topography was another important factor impacting $a_{CDOM}(400)$ distribution in the ZJE. Deep water channels were located in the east and fresh water was discharged into the west (Wang et al., 2013; Liu et al., 2015). When the tide rising, saline waters intruded into the Lingding Bay from the east channels and were advected by fresh water to form a counter-clockwise current inside the Lingding Bay (Chen et al., 2004). Consequently, the CDOM concentration was high in the west of the Lingding Bay, especially in summer when with high water discharge from the Zhujiang River (Fig. 8). The CDOM diffusion along with fresh water was also related to

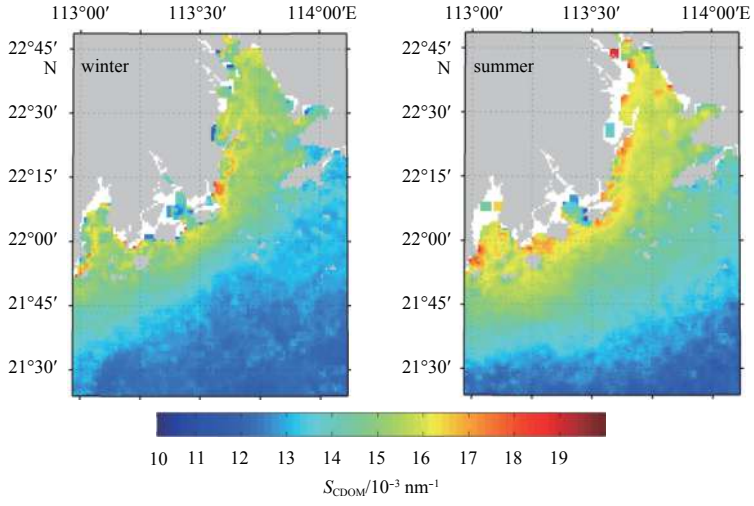

Fig. 11. Satellite-derived seasonal CDOM spectral slope in winter and summer. The same as Fig. 8, seasonal S_{CDOM} was denoted by the mean value in a specific month from 2002 to 2014. Owing to light effects from land objects, few values near the land are abnormal.

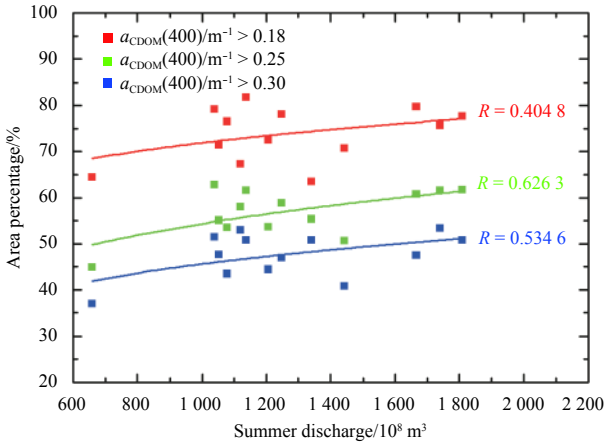

Fig. 12. Influences of discharge from the Zhujiang River on $a_{CDOM}(400)$ distribution in summer. The area percent was calculated from the satellite-derived seasonal $a_{CDOM}(400)$ as shown in Fig. 8.

water currents in the northern SCS. Outside the Lingding Bay, surface water flowed southwest along the Guangdong seacoast in winter, but northeast in summer (Dong et al., 2004; Wong et al., 2007; Bai et al., 2015). Therefore, part of high $a_{CDOM}(400)$ waters were transported eastward in summer, but westward in winter (Figs 1 and 8).

6.3 *Relationship between CDOM and DOC*

Terrigenous CDOM, although resistant to biodegradation, might be degraded to non-colored DOM or CO_2 after absorbing light in the estuary (Hernes and Benner, 2003; Hong et al., 2005; Bauer et al., 2013). Moreover, CDOM might also be decomposed through biological activities such as bacterial utilization (Amon and Benner, 1996; Hong et al., 2005), micro-zooplankton ZJEdation (Mannino et al., 2008), and virus hydrolysis (Pan et al., 2012), etc. Judging from the conservative CDOM mixing (Fig. 4a), however, these processes were not significant in the ZJE. Except for CDOM, other non-colored DOM might be labile and therefore had a short residence time (Chen et al., 2004). Furthermore, DOM from other sources might have a different non-colored DOM fraction with that from the Zhujiang River. All of these together shaped the correlation between CDOM and DOC in the ZJE.

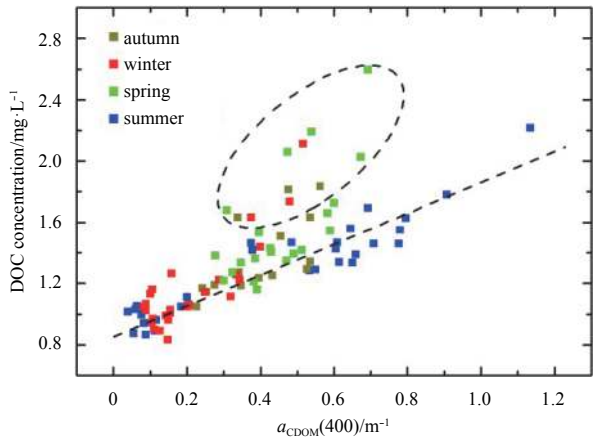

Fig. 13. Relationship between $a_{CDOM}(400)$ and the DOC concentration in the ZJE. All data, 93 in total, was from the four conducted cruises (Section 3.1). The black dash line denotes the fitted line between $a_{CDOM}(400)$ and the DOC concentration using the *in situ* data in summer cruise. The dark dash ellipse contains data apart from the dash line; relative stations are all with low salinities.

Figure 13 shows the scatter plot of $a_{CDOM}(400)$ and the DOC concentration in the ZJE. In summer with larger water discharge, fresh water stayed in the ZJE for shorter time. DOC co-varied with $a_{CDOM}(400)$, with R^2 of 0.866 6. For other three seasons, waters of some stations with low salinities had significantly high DOC concentrations (Fig. 13). There were two possible reasons for these deviations. The first one was the input of anthropogenic DOC. Several Chinese metropolises are located around the ZJE, such as the Guangzhou, Shenzhen. Industrial wastewater and domestic sewage with the high DOC concentration might be discharged into the ZJE without removing DOM well. These DOM, mainly protein, were biodegradable and easily degraded soon after being poured into the ZJE. The other one was the transformation from POC to DOC in low salinity waters. The Zhujiang River affected by the East Asian Monsoon was featured by high ratio of POC to DOC (Ni et al., 2008). During the early stage of estuarine mixing, macro-particulate might be transformed into DOM so as to increase the DOC concentration (Dai et al., 2000). These increases not only collapsed the conservative mixing of DOC, but also complicated the estimation of the effective riverine end-member DOC concentration. These might also account for the abnormally high C_e in the winter of 2004, 2005 and 2006 (Fig. 10b).

7 Conclusions and prospects

The estuarine DOM distribution and characteristic are comprehensive functions of various impact factors. A series of physical-biogeochemical processes can influence the estuarine DOM dynamics. For the ZJE, high variation and great importance to water environment make it is necessary to monitor estuarine DOM in high tempo-spatial resolution. Satellite remote sensing is a good choice. This study developed remote sensing algorithms to inverse the CDOM concentration (determined by $a_{CDOM}(400)$) and its spectral slope (S_{CDOM}) using the *in situ* R_{rs} data from four seasonal cruises in the ZJE. Then, the new developed algorithms were applied on the water reflectance of MODIS/Aqua from 2002 to 2014 to calculate seasonal $a_{CDOM}(400)$ and S_{CDOM} in the ZJE.

In the ZJE, CDOM was primarily sourced from fresh water of the Zhujiang River. These terrigenous CDOM was rich in fulvic acid, which accounted for the unexpectedly high fulvic acid fraction of CDOM in the low salinity waters. The CDOM distributions were majorly influenced by water discharge of the Zhujiang River and the underwater topography influencing water mixing. CDOM was conservatively mixed and linearly decreased with increasing salinity in the ZJE. Along Section P vertical to water depth gradient, satellite-derived seasonal $a_{CDOM}(400)$ could be described by decaying exponential functions shaped as $y=ae^{bx}$ ($b<0$), with minimum R^2 of 0.753 8 in spring and maximum R^2 of 0.971 4 in summer. Combining with water discharge measured at hydrometric stations of the Zhujiang River in summer and winter from 2002 to 2014, the effective riverine end-member DOC concentration and flux into the SCS were first estimated from the MODIS/Aqua data. In summer with great discharge, both effective riverine end-member DOC concentration and flux had significantly positive correlations with the discharge of the Zhujiang River. However, they might be overestimated due to DOM sourced from human activities and POC in winter, especially in years with abnormally low river discharge.

On the basis of conservative mixing of CDOM, the developed

CDOM algorithm can further be applied to monitor salinity distribution, the fresh water diffusion, the mass transportation, etc. in the ZJE. However, the conservative mixing of DOC was disturbed by *in situ* produced DOC in the low salinity waters, significantly in autumn and spring. After figuring out these DOC additions, the satellite estimation of the effective riverine end-member DOC concentration and flux may also be realized in these seasons. Moreover, the developed algorithms employed commonly used bands of ocean color sensors, such as the medium-resolution imaging spectrometer (MERIS), the geostationary ocean color imager (GOCI), visible infrared imaging radiometer suite (VIIRS), etc. Therefore, using global ocean color satellite data they can also be used to monitor DOM dynamics in other estuaries. The developed algorithms can be applied to explore DOM compositions, distributions, and dynamic changes, etc. in highly turbid estuaries.

Acknowledgements

The authors thank the Level 1 and Atmosphere Archive and Distribution System for providing us with the daily level 1 B calibrated radiance products of MODIS/Aqua (MYD021KM, Version 2.16). We are particularly thankful to the crews of the four seasonal cruises conducted in the Zhujiang (Pearl River) Estuary for their help of field sampling.

References

Amon R M W, Benner R. 1996. Bacterial utilization of different size classes of dissolved organic matter. Limnology and Oceanography, 41(1): 41–51

Arenz R F Jr, Lewis W M Jr, Saunders J F. 1996. Determination of chlorophyll and dissolved organic carbon from reflectance data for Colorado reservoirs. International Journal of Remote Sensing, 17(8): 1547–1566

Bai Yan, Pan Delu, Cai Weijun, et al. 2013. Remote sensing of salinity from satellite-derived CDOM in the Changjiang River dominated East China Sea. Journal of Geophysical Research: Oceans, 118(1): 227–243

Bai Yan, He Xianqiang, Pan D, et al. 2014. Summertime Changjiang River plume variation during 1998–2010. Journal of Geophysical Research: Oceans, 119(9): 6238–6257

Bai Yan, Huang T H, He Xianqiang, et al. 2015. Intrusion of the Pearl River plume into the main channel of the Taiwan Strait in summer. Journal of Sea Research, 95: 1–15

Bailey S W, Werdell P J. 2006. A multi-sensor approach for the on-orbit validation of ocean color satellite data products. Remote Sensing of Environment, 102(1–2): 12–23

Bauer J E, Cai W J, Raymond P A, et al. 2013. The changing carbon cycle of the coastal ocean. Nature, 504(7478): 61–70

Belanger S, Babin M, Larouche P. 2008. An empirical ocean color algorithm for estimating the contribution of chromophoric dissolved organic matter to total light absorption in optically complex waters. Journal of Geophysical Research: Oceans, 113(C4): C04027

Cai Wei-Jun, Dai Minhan, Wang Yongchen, et al. 2004. The biogeochemistry of inorganic carbon and nutrients in the Pearl River estuary and the adjacent northern South China Sea. Continental Shelf Research, 24(12): 1301–1319

Cai Wei-Jun, Guo Xianghui, Chen C T A, et al. 2008. A comparative overview of weathering intensity and HCO3- flux in the world's major rivers with emphasis on the Changjiang, Huanghe, Zhujiang (Pearl) and Mississippi Rivers. Continental Shelf Research, 28(12): 1538–1549

Callahan J, Dai Minhan, Chen R F, et al. 2004. Distribution of dissolved organic matter in the Pearl River Estuary, China. Marine Chemistry, 89(1–4): 211–224

Carder K L, Chen F R, Lee Zhongping, et al. 2003. MODIS Ocean Science Team-Algorithm Theoretical Basis Document. ATBD 19, Case 2 Chlorophyll a, Version 7. NASA MODIS

Carder K L, Steward R G, Harvey G R, et al. 1989. Marine humic and fulvic acids: Their effects on remote sensing of ocean chlorophyll. Limnology and Oceanography, 34(1): 68–81

Chen Chuqun, Shi Ping, Zhan Haigang. 2003. A local algorithm for estimation of yellow substance (gelbstoff) in coastal waters from SeaWiFS data: Pearl River estuary, China. International Journal of Remote Sensing, 24(5): 1171–1176

Chen Hao, Meng Wei, Zheng Bing-Hui, et al. 2013. Optical signatures of dissolved organic matter in the watershed of a globally large river (Yangtze River, China). Limnologica-Ecology and Management of Inland Waters, 43(6): 482–491

Chen Zhiqiang, Li Yan, Pan Jianming. 2004. Distributions of colored dissolved organic matter and dissolved organic carbon in the Pearl River Estuary, China. Continental Shelf Research, 24(16): 1845–1856

Dai Minhan, Martin J M, Hong Huasheng, et al. 2000. ZJEliminary study on the dissolved and colloidal organic carbon in the Zhujiang River estuary. Chinese Journal of Oceanology and Limnology, 18(3): 265–273

Dai Minhan, Yin Zhiqiang, Meng Feifei, et al. 2012. Spatial distribution of riverine DOC input to the ocean: an updated global system. Current Opinion in Environmental Sustainability, 4(2): 170–178

Dong Lixian, Su Jilan, Wong L A, et al. 2004. Seasonal variation and dynamics of the pearl river plume. Continental Shelf Research, 24(16): 1761–1777

Dong Qiang, Shang Shaoling, Lee Zhongping. 2013. An algorithm to retrieve absorption coefficient of chromophoric dissolved organic matter from ocean color. Remote Sensing of Environment, 128: 259–267

D'Sa E J, Miller R L. 2003. Bio-optical properties in waters influenced by the Mississippi River during low flow conditions. Remote Sensing of Environment, 84(4): 538–549

Fang Ligang, Chen Shuisen, Li Dong, et al. 2009. Use of reflectance ratios as a proxy for coastal water constituent monitoring in the pearl river estuary. Sensors, 9(1): 656–673

Gao Q, Tao Z, Shen C, et al. 2002. Riverine organic carbon in the Xijiang River (South China): seasonal variation in content and flux budget. Environmental Geology, 41(7): 826–832

Guo Weidong, Yang Liyang, Zhai Weidong, et al. 2013. Runoff-mediated seasonal oscillation in the dynamics of dissolved organic matter in different branches of a large bifurcated estuary-The Changjiang Estuary. Journal of Geophysical Research: Biogeosciences, 119(5): 776–793

He Biyan, Dai Minhan, Zhai Weridong, et al. 2010. Distribution, degradation and dynamics of dissolved organic carbon and its major compound classes in the Pearl River Estuary, China. Marine Chemistry, 119(1–4): 52–64

He Xianqiang, Bai Yan, Pan Delu, et al. 2013. Using geostationary satellite ocean color data to map the diurnal dynamics of suspended particulate matter in coastal waters. Remote Sensing of Environment, 113: 225–239

Hernes P J, Benner R. 2003. Photochemical and microbial degradation of dissolved lignin phenols: Implications for the fate of terrigenous dissolved organic matter in marine environments. Journal of Geophysical Research: Oceans, 108(C9): 3291

Hong Huasheng, Wu Jingyu, Shang Shaoling, et al. 2005. Absorption and fluorescence of chromophoric dissolved organic matter in the Pearl River Estuary, South China. Marine Chemistry, 97(1–2): 78–89

Huang Wei, Chen R F. 2009. Sources and transformations of chromophoric dissolved organic matter in the Neponset River Watershed. Journal of Geophysical Research: Biogeosciences, 114(G4): G00F05

Jaffé R, Boyer J N, Maie N, et al. 2004. Source characterization of dissolved organic matter in a subtropical mangrove-dominated estuary by fluorescence analysis. Marine Chemistry, 84(3–4): 195–210

Knap A H, Michaels A F, Close A R, et al. 1996. Protocols for the joint global ocean flux study (JGOFS) core measurements. Jgofs.

Lee Zhongping, Carder K L, Arnone R A. 2002. Deriving inherent optical properties from water color: a multiband quasi-analytical algorithm for optically deep waters. Applied Optics, 41(27): 5755–5772

Liu Dong, Pan Delu, Bai, Yan, et al. 2015. Remote Sensing Observation of Particulate Organic Carbon in the Pearl River Estuary. Remote Sensing, 7(7): 8683–8704

Liu Qiong, Pan Delu, Bai Yan, et al. 2014. Estimating dissolved organic carbon inventories in the East China Sea using remote-sensing data. Journal of Geophysical Research: Oceans, 119(10): 6557–6574

Mannino A, Russ M E, Hooker S B. 2008. Algorithm development and validation for satellite-derived distributions of DOC and CDOM in the US Middle Atlantic Bight. Journal of Geophysical Research: Oceans, 113(C7): C07051

Mitchell B G, Kahru M, Wieland J, et al. 2000. Determination of spectral absorption coefficients of particles, dissolved material and phytoplankton for discrete water samples, In: Fargion G S Mueller J, eds. Ocean Optics Protocols for Satellite Ocean Color Sensor validation., Goddard Space Flight Space Center, Greenbelt, Md

Mueller J L, Fargion G S, Mcclain C R. 2003. Biogeochemical and bio-optical measurements and data analysis methods, NASA Tech. Mem., NASA TM-2003-211621, Rev. 4, vol. 2, Goddard Space Flight Space Center, Maryland

Ni Honggang, Lu Feng-Hui, Luo Xian-Lin, et al. 2008. Riverine inputs of total organic carbon and suspended particulate matter from the Pearl River Delta to the coastal ocean off South China. Marine Pollution Bulletin, 56(6): 1150–1157

Pan Delu, Liu Qiong, Bai Yan. 2012. Progress in remote sensing of DOC: based on the analysis of conservative behaviors of DOC and CDOM in global large rivers estuaries. Haiyang Xuebao (in Chinese), 34(4): 1–11

Park Y, Ahn Y, Han H, et al. 2014. GOCI level 2 Ocean Color Products (GDPS 1.3) Brief Algorithm Description. 17 November

Ran Lishan, Lu X X, Sun Huiguo, et al. 2013. Spatial and seasonal variability of organic carbon transport in the Yellow River, China. Journal of Hydrology, 498: 76–88

IOCCG. 2000. Remote sensing of ocean colour in coastal, and other optically-complex, waters. Sathyendranath, S. (ed.), reports of the international ocean-colour coordinating group, No. 3, IOCCG, Dartmouth, Canada.

Siegel D A, Maritorena S, Nelson N B, et al. 2002. Global distribution and dynamics of colored dissolved and detrital organic materials. Journal of Geophysical Research: Oceans, 107(C12): 21-1–21-14

Siswanto E, Tang J, Yamaguchi H, et al. 2011. Empirical ocean-color algorithms to retrieve chlorophyll-α, total suspended matter, and colored dissolved organic matter absorption coefficient in the Yellow and East China Seas. Journal of Oceanography, 67(5): 627–650

Sun Jian, Lin Binliang, Li Kaiming, et al. 2014. A modelling study of residence time and exposure time in the Pearl River Estuary, China. Journal of Hydro-environment Research, 8(3): 281–291

Świrgoń M, Stramska M. 2015. Comparison of *in situ* and satellite ocean color determinations of particulate organic carbon concentration in the global ocean. Oceanologia, 57(1): 25–31

Tiwari S P, Shanmugam P. 2011. An optical for the remote sensing of coloured dissolved organic matter in coastal/ocean waters. Estuarine, Coastal and Shelf Science, 93(4): 396–402

Wang Menghua, Shi Wei. 2007. The NIR-SWIR combined atmospheric correction approach for MODIS ocean color data processing. Optics ExZJEss, 15(24): 15722–15733

Wang Xuchen, Ma Haiqing, Li Ronghua, et al. 2012. Seasonal fluxes and source variation of organic carbon transported by two major Chinese rivers-The Yellow River and Changjiang (Yangtze) River. Global Biogeochemical Cycles, 26(2): GB2025

Wang Xiaozhen, Zhang Huaguo, Fu Bin, et al. 2013. Analysis on the coastline change and erosion-accretion evolution of the Pearl River Estuary, China, based on remote-sensing images and nautical charts. Journal of Applied Remote Sensing, 7: 073519

Wong G T F, Ku T, Mulholland M, et al. 2007. The South East Asian time-series study (SEATS) and the biogeochemistry of the South China Sea—An overview. Deep-Sea Research II: Topical Studies in Oceanography, 54(14–15): 1434–1447

Wu Y, Zhang J, Liu S M, et al. 2007. Sources and distribution of carbon within the Yangtze River system. Estuarine, Coastal and Shelf Science, 71(1–2): 13–25

Xing Xiaogang, Zhao Dongzhi, Liu Yuguang, et al. 2008. Absorption characteristics of de-pigmented particle and yellow substance in Bohai Sea. Marine Environmental Science (in Chinese), 27(6): 595–598

Yu Mengde, Bai Jinquan. 1962. Effect of vegetation on the composition of humus and active mineral substences in soils of Kwangtung and Kwangsi. Acta Pedologica Sinica (in Chinese), 10(1): 29–43

Zhu Weining, Yu Qian, Tian Y Q, et al. 2011. Estimation of chromophoric dissolved organic matter in the Mississippi and Atchafalaya river plume regions using above-surface hyperspectral remote sensing. Journal of Geophysical Research: Atmospheres, 116(C2): C02011